Incomplete fusion in $^{16}O + {}^{89}Y$ reactions at energies of ≈ 7 MeV/nucleon

Muntazir Gull,[1,*] Kamal Kumar,[1] Sabir Ali,[2,†] Tauseef Ahmad,[1] S. Dutt,[1] I. A. Rizvi,[1] Avinash Agarwal,[3] and R. Kumar[4]

[1]*Department of Physics, Aligarh Muslim University, Aligarh, Uttar Pradesh 202 002, India*
[2]*MANUU Polytechnic Darbhanga, Maulana Azad National Urdu University, Hyderabad 500 032, India*
[3]*Department of Physics, Bareilly College, Bareilly, Uttar Pradesh 243 005, India*
[4]*NP-Group, Inter University Accelerator Centre, New Delhi 110 067, India*

Measurement of forward recoil range distribution (FRRD) of evaporation residues (ERs) populated in the $^{16}O + {}^{89}Y$ reaction at $E_{lab} \approx 105$ MeV have been carried out by employing the offline characteristic γ-ray detection method. The FRRD pattern of ERs populated through xn/pxn channels comprises a single peak only whereas ERs populated through α emitting channel have multiple peaks in their FRRD. FRRDs of the observed ERs support the presence of the complete fusion (CF) process in the population of xn/pxn channels residues and an admixture of complete and incomplete fusion (ICF) processes in the population of α emitting channel residues. The observed ICF process in the population of α emitting channel residues is explained through the breakup fusion model. The fusion function is derived from the experimental CF cross section data and the extracted fusion function is compared with the universal fusion function to estimate the degree of ICF contribution to the total fusion cross section. An attempt has also been made to explore the dependence of ICF probability on target charge.

I. INTRODUCTION

It is now a well established fact that several reaction mechanisms are active in reactions induced by light-heavy projectiles ($5 \leqslant Z \leqslant 10$) at energies well above the Coulomb barrier [1–3]. These possible reaction mechanisms can be classified on the basis of quantum of linear momentum transferred from the incident projectile to the resulting compound system. The incident projectile may fuse with the target nucleus as a single entity, leading to a complete transfer of momentum to the resulting compound system through the direct complete fusion (DCF) process. On the other hand, the incident projectile may break up into fragments in the periphery of the target's nuclear field, opening a chain of new reaction channels. If all the breakup fragments of the incident projectile fuse with the target nucleus, one after the other, the process is called sequential complete fusion (SCF). It is also possible that only a part of the incident projectile fuses with the target nucleus through the incomplete fusion (ICF) process. There is also possibility that none of the breakup fragments of the incident projectile are able to fuse with the target nucleus, leading to the noncapture breakup (NCBU) process. Both SCF and DCF processes lead to the formation of the same compound nucleus with the same excitation energy and momentum transferred, making it difficult to differentiate between the two processes. Thus only the complete fusion (CF) cross section, which is the algebraic sum of SCF and DCF, i.e., $\sigma_{CF} = \sigma_{SCF} + \sigma_{DCF}$, can be measured experimentally.

In heavy ion induced reactions at laboratory energy ≈ 7 MeV/nucleon, CF and ICF processes were found to be the most dominant among all the possible reaction channels. It was reported by Britt and Quinton [4] that partial linear momentum transfer in heavy ion induced reactions at energy well above the Coulomb barrier is accompanied by forward emitted fast light particles. The production of these fast light particles has been attributed to the breakup of the incident projectile in the periphery of the target nucleus. Since the first observation of forward emitted fast particles [4], the breakup process has been studied for many systems [5,6]. However, a consistent appreciation of the projectile breakup process, now referred to as ICF, only emerged with the work of Inamura *et al.* [7] by employing the particle/γ coincidence measurement of the projectile-like fragment. Following the breakup of the incident projectile under the influence of target's field, one of the fragments, called the *spectator*, continues almost undeflected along the beam direction with the same velocity as that of the incident beam, while the remaining fragment fuses with the target nuclei leading to a partial transfer of incident linear momentum from the projectile to the resulting compound system.

The contribution of the ICF cross section to the total fusion (TF) cross section, which is the algebraic sum of CF and ICF, i.e., $\sigma_{TF} = \sigma_{CF} + \sigma_{ICF}$, was found to be influenced by various entrance channel parameters such as projectile structure, mass asymmetry, breakup threshold energy of the incident projectile ($E_{B.U.}$), etc. It was predicted theoretically [8] and later on confirmed experimentally [9–11] that the CF cross section in heavy ion induced reaction decreases at energies well above the Coulomb barrier while the TF cross section continue to increase with the increase in beam energy.

*muntazirgull1@gmail.com
†sabir@manuu.ac.in

This systematics of CF and TF was considered by many authors [12,13] to be a consequence of the critical angular momentum ℓ_{crt} associated with the formation of a compound system; i.e., at angular momenta ℓ higher than ℓ_{crt} for CF, compound nucleus formation is hindered and the ICF reaction starts competing with the CF.

In order to explain the forward emitted fast light particle spectra observed in ICF reactions, the breakup fusion model was proposed by Udagawa and Tamura [14]. Another such model, called the sum rule model, was proposed by Wilczynski *et al.* [15]. The sum rule model, which envisages the localization of the different ICF channels in the angular momentum space above the ℓ_{crt} for CF, explains very well the ICF cross section at energies above 10 MeV/nucleon, but at lower energies it underestimates the ICF cross sections. A few studies, particularly those involving spherical targets, have shown the involvement of angular momenta much lower than ℓ_{crt} in the ICF reactions [16]. Morgenstern *et al.* found ICF channels in the velocity spectra of evaporation residues (ERs) in the reaction of ^{40}Ar with boron and carbon targets [17]. Tserruya *et al.* noticed the evidence of ICF using the time-of-flight technique at 5.5–10 MeV/nucleon energy in the reaction of ^{12}C with ^{120}Sn, ^{160}Gd, and ^{197}Au targets [18].

Various ERs populated in heavy ion induced reaction at $E_{lab} \approx 7$ MeV were likely to have contributions arising from CF and/or ICF processes. The extent of CF and/or ICF contribution to the TF cross section varies from residue to residue. So far there is no theoretical model proposed which can predict the degree of contribution arising from CF and/or ICF processes in the population of a given ER. However, experimentally this can be achieved either by directly observing the residues using the particle/γ coincidence measurement [19] or by measuring the forward recoil range distribution (FRRD) of the populated ER in a stopping medium, which has been utilized in the present work. Thus, in order to estimate the degree of contribution arising from CF and/or ICF processes in the population of a given ER, the present work was carried out. The main objective of the present work is to study the role of various entrance channel parameters on fusion incompleteness by measuring the FRRDs of the ERs populated in ^{16}O + ^{89}Y reaction at $E_{lab} \approx 105$ MeV. Experimental details related to the present work are given in Sec. II, whereas details of result analysis are given in Sec. III. Finally the conclusions of the present work are discussed in Sec. IV.

II. EXPERIMENTAL DETAILS

A. Target preparation and irradiation

The experiment was performed at the Inter University Accelerator Centre (IUAC), New Delhi, India using a ^{16}O^{7+} beam at $E_{lab} \approx 105$ MeV from the 15UD accelerator. Target foil was placed in the form of a stack comprising the ^{89}Y target followed by a series of Al-catcher foils for trapping the recoiling ERs. The ^{89}Y target foil of thickness 200 μg/cm^2, evaporated on Al backing of thickness 1.92 mg/cm^2, was used for irradiation. The combination of ^{89}Y target foil and Al backing was placed normal to the beam axis such that the Al backing faced the incident beam followed by a stack of 14 thin
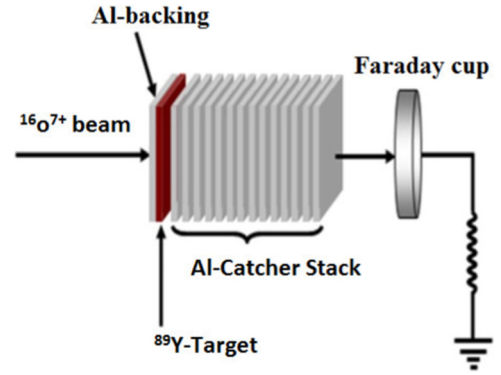

FIG. 1. A schematic diagram of target-catcher foil arrangement used for the study of the forward recoil range distribution of ERs populated in the ^{16}O + ^{89}Y reaction at $E_{lab} \approx 105$ MeV.

Al catcher foils. The thickness of the Al catcher foils ranged from 93 to 144 μg/cm^2. The thickness of each Al catcher and target foil had been determined prior to use by weighing as well as by the α transmission method. The thicknesses of Al catcher foils were chosen in such a manner that the recoil range of the heaviest populated ER fell within the cumulative thickness of the Al catcher foils. The ^{16}O^{7+} beam was collimated to a spot of diameter 8 mm and the stack was irradiated with beam current varying between $\approx$ 25 and 30 nA for $\approx$ 9 h, keeping in mind the half-lives of the populated ERs. Beam current was measured behind the target-catcher assembly with an electron suppressed Faraday cup, using a current integrator device. A schematic diagram of target-catcher foil arrangement used in the present work is shown in Fig. 1. The irradiation of the stack comprising the target-catcher foil assembly was carried out in the General Purpose Scattering Chamber (GPSC), which has an in-vacuum transfer facility to minimize the lapse time between the termination of the irradiation and beginning of the counting of induced activity.

B. Post-irradiation analysis and identification of the residues

Following the irradiation, counting of activity of the populated ERs trapped in different catcher foils was carried out using a high purity germanium (HPGe) detector having an active volume of 100 cc coupled to a computer-automated measurement and control (CAMAC) based data acquisition system. Prior to counting of the induced activity, the HPGe detector was calibrated using standard γ-ray source ^{152}Eu. The γ-ray activities of the populated ERs were recorded several times starting immediately after the stopping of beam current and continuing for few days, at intervals ranging from 15 minutes to several hours. The resolution of the HPGe detector was found to be 2.5 keV for a 1408 keV γ ray from ^{152}Eu source. The activity of observed residues populated in the ^{16}O + ^{89}Y reaction at $E_{lab} \approx 105$ MeV, listed in Table I, were extracted from the recorded γ-ray spectra. A typical γ-ray energy spectrum of the ERs populated in the ^{16}O + ^{89}Y reaction at $E_{lab} \approx 105$ MeV recorded for 100 seconds, 15 minutes after the termination of the irradiation, is shown in Fig. 2. Various peaks observed in the recorded γ-ray spectrum were assigned to different ERs, populated in the course of

TABLE I. Observed ERs, populated through different reaction channels in the ^{16}O + ^{89}Y reaction at $E_{lab} \approx 105$ MeV, are given in the first column along with their half lives in the second column, and other columns have spectroscopic properties taken from Ref. [20].

Reaction	Half-life	J^{π}	E_{γ} (keV)	I^{γ}
^{89}Y(^{16}O, $4n$)^{101}Ag	11.1 min	$9/2^+$	260.9	53.0
			588.0	10.05
^{89}Y(^{16}O, $p3n$)^{101}Pd	8.47 h	$5/2^+$	296.9	19.0
			590.4	12.0
^{89}Y(^{16}O, $p5n$)^{99}Pd	21.4 min	$5/2^+$	136.0	73.0
			263.6	15.2
^{89}Y(^{16}O, αn)^{100g}Rh	20.8 h	1^-	539.5	80.6
			822.6	21.0
			1107.0	13.5
^{89}Y(^{16}O, $\alpha 2n$)^{99m}Rh	4.7 h	$9/2^+$	340.7	70.0
			617.8	12.0
^{89}Y(^{16}O, $\alpha 3n$)^{98}Rh	8.7 min	2^+	652.4	94.0
			745.4	5.4
^{89}Y(^{16}O, $2\alpha 2n$)^{95g}Tc	4.06 h	$9/2^+$	765.7	93.8
^{89}Y(^{16}O, $2\alpha 3n$)^{94g}Tc	4.88 h	7^+	871.1	100.0

FIG. 3. Half-life decay curve of (a) ^{94g}Tc (4.88 h) and (b) ^{101}Ag (11.1 min) residues populated in the ^{16}O + ^{89}Y reaction at $E_{lab} \approx 105$ MeV.

irradiation, on the basis of their characteristic γ rays as well as by their measured half-lives. The measured half-lives of the observed ERs were found to be in good agreement with their literature values taken from Ref. [20]. As a representative case the half-life decay curves of the ^{94g}Tc and ^{101}Ag residues, having half-lives of 4.88 hours and 11.1 minutes, respectively, are shown in Fig. 3.

The reaction cross sections of the observed ERs populated through different fusion processes were calculated using the standard formulation [21] given by

$$\sigma_r = \frac{A\lambda \exp(\lambda t_2)}{N_0 \theta \phi \epsilon_G K[1 - \exp(-\lambda t_1)][1 - \exp(-\lambda t_3)]}, \quad (1)$$

where A is the total number of counts recorded under the peak in time t_3, λ is the decay constant of the product nucleus, N_0 is the total number of nuclei present in the target foil, θ is the branching ratio of the identified γ ray, ϕ is the incident beam particle flux, ϵ_G is the geometry-dependent efficiency
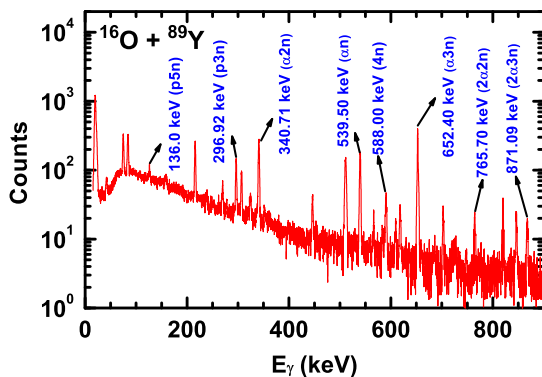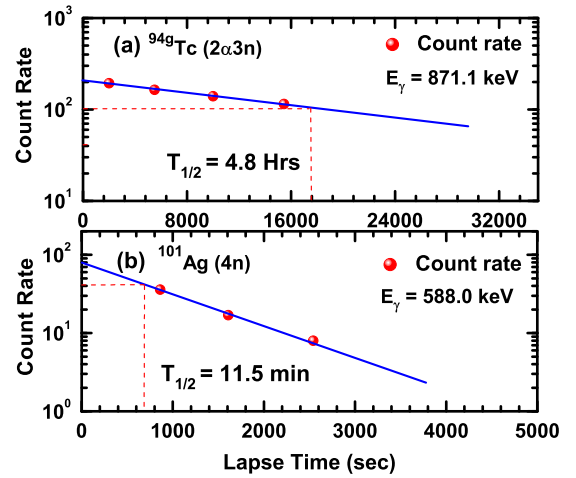

FIG. 2. Typical γ-ray energy spectrum of the residues populated in the ^{16}O + ^{89}Y reaction at $E_{lab} \approx 105$ MeV recorded for 100 seconds, 15 minutes after the termination of the irradiation.

of the HPGe detector, t_1 is the irradiation time of the stack, t_2 is the time elapsed between the termination of the irradiation and the start of the counting, t_3 is the counting time, and $K = [1 - e^{-\mu d}]/\mu d$ is the self-absorption correction factor for the target material of thickness d with the absorption coefficient μ. The correction factor for the decay of the induced activity due to the delay time t_2 between the stop of irradiation and the start of counting is taken as $[\exp(\lambda t_2)]$ and the correction factor due to the decay of the irradiated sample during the data accumulation time t_3 is taken as $[1 - \exp(-\lambda t_3)]$. During the irradiation, a factor $[1 - \exp(-\lambda t_1)]$ takes care of the decay of ERs and is known as the saturation correction factor. Further details regarding the experimental setup and cross section measurement are given in Ref. [22].

Error and uncertainty in measured reaction cross section of the observed ERs were likely to arise from different possible sources. Some of the potential sources of error in the present work are as follows: (i) Nonuniformity in the target thickness leads to an uncertainty in determining the number of target nuclei. In order to check the uniformity of the target and catcher foils, the thickness of each target and catcher foil was measured at different positions by α transmission method. The error arising due to the uncertainty in thickness of target foil was found to be less than 3%. (ii) The error arising due to the geometry dependent detector efficiency, caused by the statistical uncertainty in the counts under the peak, was estimated to be less than 5%. (iii) The error contributed due to the dead time of the spectrometer was kept below 10% by suitably adjusting the sample-detector separation. (iv) Fluctuation in beam current leads to variation in the flux of incident projectile beam. Proper care was taken to keep the beam current constant. The error arising due to the fluctuation in the beam current was found to be less than 3%. (v) The error associated with the energy straggling of the ion beam was estimated to be less than 2%. During the experiment much effort was made to minimize the errors in experimentally measured reaction cross sections of the populated ERs, which

in the present work are estimated to be around 15%, but this excludes the error arising due to the branching ratio and decay constant.

III. RESULTS ANALYSIS AND INTERPRETATION

In order to have a glimpse of the different fusion processes involved in the population of ERs in the ^{16}O + ^{89}Y reaction at $E_{\mathrm{lab}} \approx 105$ MeV, measurements of FFRD of the observed residues were carried out. At $E_{\mathrm{lab}} \approx 105$ MeV, a total of eight ERs, namely ^{101}Ag ($4n$), ^{101}Pd ($p3n$), ^{99}Pd ($p5n$), ^{100g}Rh (αn), ^{99m}Rh ($\alpha 2n$), ^{98}Rh ($\alpha 3n$), ^{95g}Rh ($2\alpha 2n$), and ^{94g}Rh ($2\alpha 3n$) were found to get populated through different fusion processes in the ^{16}O + ^{89}Y reaction. Among the observed ERs, residues populated through α-emitting channels (^{100g}Rh, ^{99m}Rh, ^{98}Rh, ^{95g}Rh, ^{94g}Rh) were likely to get populated through the CF as well ICF processes. On the other hand, residues populated through xn/pxn channels (^{101}Ag, ^{101}Pd, ^{99}Pd) have the possibility of getting populated through the CF process only.

ERs populated through the CF and/or ICF processes pass through an intermediate stage in which an excited intermediate compound system is formed through the partial or total amalgamation of the incident projectile with the target nucleus. In case of CF, the intermediate compound system recoils along the beam direction with a velocity and excitation energy governed totally by the energy and momentum of the incident projectile, whereas in the case of the ICF process the intermediate compound system formed at a given incident energy is populated with an extended distribution of recoil velocity, recoil angle, and excitation energy [23].

A. Forward recoil range distribution

The use of the forward recoil range distribution (FRRD) technique in the study of nuclear reactions can provide detailed information about the reaction mechanism of different fusion processes involved in the population of ERs. For a particular reaction, measurement of recoil velocity of the heavy products or, equivalently, its FRRD in some stopping medium, can be used to determine the degree of momentum transferred from the incident projectile to the resulting compound system. Careful measurement of FRRD of the populated ERs is a powerful tool in distinguishing between the different ICF processes in lighter systems, such as the present one, where the same product may be populated by more than one fusion process, followed by different degrees of charged particle evaporation.

The projected FRRD, which reflects the velocity distribution of the populated ERs recoiling in the catcher medium, is obtained by dividing the measured yield in each catcher foil by the thickness of the corresponding catcher foil. The normalized yield thus obtained is plotted against the cumulative thickness of the Al catcher foils. ERs originating from an intermediate compound system recoil in the Al catcher medium with a well define velocity v_0. The velocity distribution of the ER is symmetric about v_0 with a width governed totally by the number of nucleons and/or α particles emitted by the recoiling intermediate compound system. For an intermediate compound system formed through the CF process, the recoil velocity of the intermediate compound system v_0 derived from the conservation of linear momentum is given as

$$v_0 = V_{\mathrm{CN}} = \frac{\sqrt{2mE}}{M}, \qquad (2)$$

where m is the incident projectile mass, M is the mass of the intermediate compound system, and E is the incident beam energy in the laboratory frame. The recoil velocity of an intermediate compound system formed through the ICF process will be less than v_0 because a fraction of the incident linear momentum p_{inc} is carried away by the spectator. If the incident projectile is assumed to be a point object, p_{inc} will be shared between the fusing fragment and spectator in a ratio proportional to their masses. Moreover, since the diameter of the incident projectile is extended over a range of impact parameters and, in general, the spectator is assumed to be breakup from the outer region of the incident projectile, the linear momentum endowed to the intermediate compound system, by a fusing fragment of mass M_f emerging from an incident projectile having mass M_p and linear momentum p_{inc}, is equal to $(M_f/M_p)p_{\mathrm{inc}}$.

1. FRRD of evaporation residues populated through xn and pxn channels

In the ^{16}O + ^{89}Y reaction at $E_{\mathrm{lab}} \approx 105$ MeV a total of three ERs, namely ^{101}Ag and ^{101,99}Pd were observed to be populated through the xn ($x = 4$) and pxn ($x = 3, 5$) channels, respectively. These xn and pxn channel ERs stem from the excited intermediate compound system ^{105}Ag* formed through the total amalgamation of the incident projectile ^{16}O with the ^{89}Y target. As a representative case, the systematics for the formation of ^{101}Pd through the $p3n$ channel may be given as

$$^{16}\mathrm{O} + {}^{89}\mathrm{Y} \Rightarrow {}^{105}\mathrm{Ag}^*,$$
$$^{105}\mathrm{Ag}^* \Rightarrow {}^{101}\mathrm{Pd} + p3n,$$
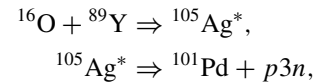
Figures 4(a)–4(c) show the FRRD of the ERs ^{101}Ag, ^{101}Pd, and ^{99}Pd populated through $4n$, $p3n$, and $p5n$ channels, respectively. As can be inferred from Figs. 4(a)–4(c), the FRRD of ERs populated through the xn ($x = 4$) and pxn ($x = 3, 5$) channels comprise a single peak only, suggesting the formation of the excited intermediate compound system ^{105}Ag* through a process involving total transfer of incident linear momentum via the complete amalgamation of the incident projectile with the target nucleus. The experimentally measured range integrated cross section along with the theoretically calculated CF cross section using the statistical model code PACE4 [24] as well as Q value and threshold energy (E_{thr}) of the observed ERs populated in the ^{16}O + ^{89}Y reaction at $E_{\mathrm{lab}} \approx 105$ MeV are given in Table II.

2. FRRD of evaporation residues populated through α emitting channels

In the ^{16}O + ^{89}Y reaction at $E_{\mathrm{lab}} \approx 105$ MeV, a total of five ERs, namely ^{100g}Rh, ^{99m}Rh, ^{98}Rh, ^{95g}Tc, and ^{94g}Tc were
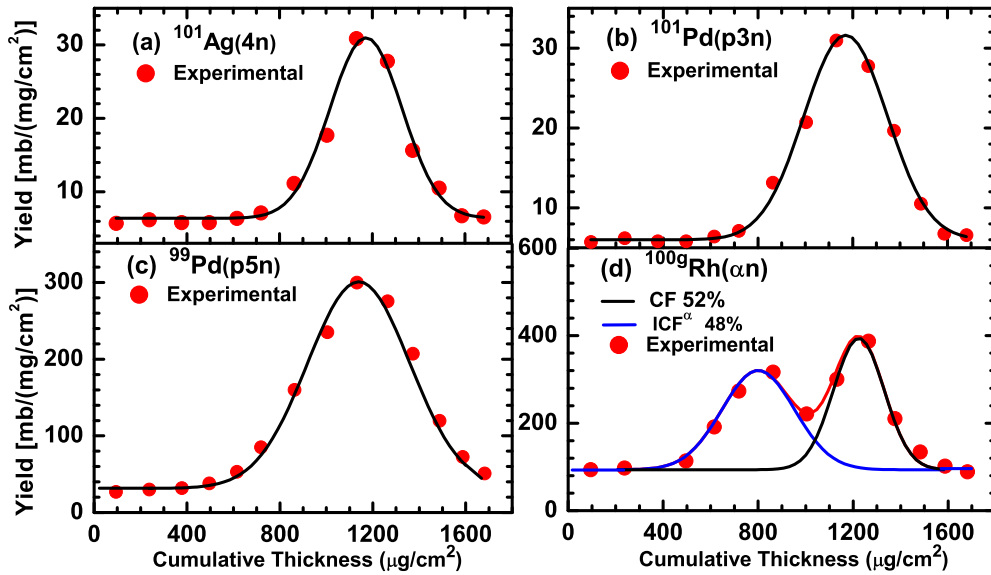
FIG. 4. Experimentally measured FRRD of ERs (a) ^{101}Ag, (b) ^{101}Pd, (c) ^{99}Pd, and (d) ^{100g}Rh populated through $4n$, $p3n$, $p5n$, and αn channels, respectively. The solid lines through the data points are the Gaussian fits of the experimental data points (solid circles).

found to get populated through the α emitting channels. ERs evolving through the α emitting channels have the possibility of getting populated through the CF as well as ICF processes, which is reflected clearly from their FRRD. ERs populated through the α emitting channels have multiple peaks in their FRRD, and each peak of the FRRD signifies a different fusion process. The contribution arising from CF and/or ICF processes in the population of α emitting channel residues can be evaluated from the area under the peak corresponding to the given fusion process. The degree of contribution arising from CF and/or ICF processes varies from residue to residue, and for a specific residue it varies with the excitation energy of the compound system. Particular interesting is the FRRD of the ER ^{95g}Tc populated through the $2\alpha2n$ channel in ^{16}O + ^{89}Y reaction at $E_{\mathrm{lab}} \approx 105$ MeV, reflecting the the interplay between CF, ICF$^{\alpha}$, and ICF$^{2\alpha}$ processes.

(1) CF process. The CF process involves the fusion of ^{16}O projectile as a single entity with the ^{89}Y target, leading to the formation of the excited intermediate compound system ^{105}Ag*. The excited intermediate compound system ^{105}Ag* further decays via the $2\alpha2n$ channel leading to the formation of ER ^{95g}Tc. Figures 4(d) and 5(a)–5(d) show the FRRD of ERs ^{100}Rh, ^{99m}Rh, ^{98}Rh, ^{95g}Tc, and ^{94g}Tc populated through the α emitting channels. As can be seen from Fig. 5(c), the FRRD of ^{95g}Tc comprises three peaks, suggesting the presence of CF, ICF$^{\alpha}$, and ICF$^{2\alpha}$ processes in the population of ^{95g}Tc. Complete amalgamation of the incident projectile with the target nucleus leads to total linear momentum transfer (LMT) from the incident projectile to the resulting compound system. The excited intermediate compound system, on acquiring the total incident linear momentum, recoils along the beam direction up to maximum depth in the Al catcher medium. The peak at the highest recoil range in the FRRD of

TABLE II. Experimentally measured range integrated as well as theoretically calculated CF cross section (PACE4) σ_{RRD} (mb) of the observed ERs populated in the ^{16}O + ^{89}Y reaction at $E_{\mathrm{lab}} \approx 105$ MeV along with the Q value (MeV) and threshold energy E_{thr} (MeV) for the CF, ICF$^{\alpha}$, and ICF$^{2\alpha}$ processes.

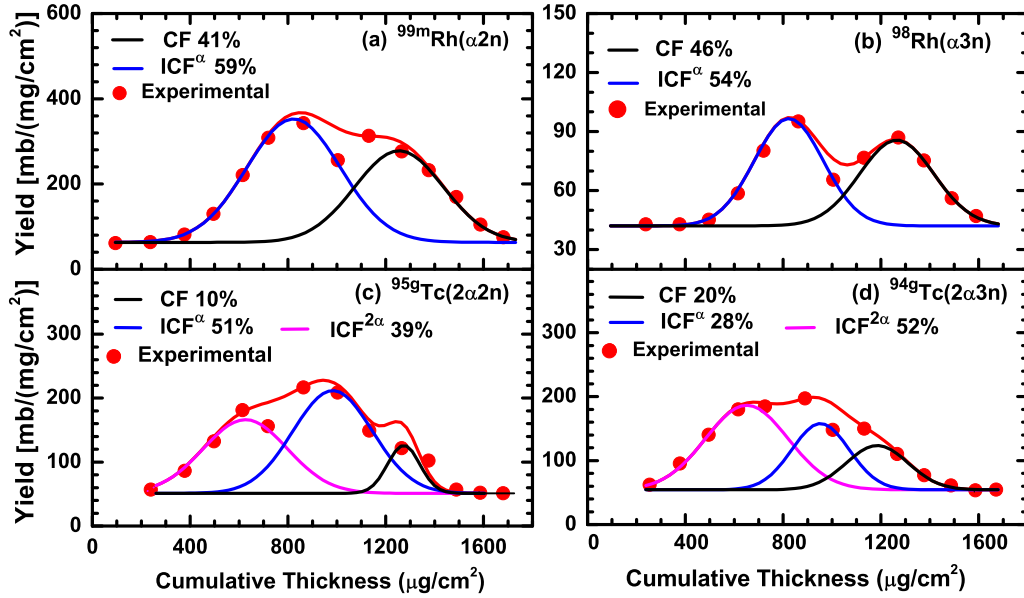| Residue	σ_{RRD} (mb)		Q value (MeV)			E_{thr} (MeV)		
	PACE4	Expt.	CF	ICF$^{\alpha}$	ICF$^{2\alpha}$	CF	ICF$^{\alpha}$	ICF$^{2\alpha}$
^{101}Ag ($4n$)	9.7	12.57 ± 1.1	-43.4			51.2		
^{101}Pd ($p3n$)	11.2	28.50 ± 3.2	-38.5			45.4		
^{99}Pd ($p5n$)	156.2	175.6 ± 12.9	-57.9			68.3		
^{100g}Rh (αn)	66.4	80.3 ± 9.6	-17.3	-10.2		20.5	11.6	
^{99m}Rh ($\alpha2n$)	85.4	97.5 ± 6.4	-25.4	-18.3		29.9	20.7	
^{98}Rh ($\alpha3n$)	21.7	16.2 ± 2.3	-35.9	-28.7		42.3	32.6	
^{95g}Tc ($2\alpha2n$)	10.3	12.5 ± 1.5	-27.5	-20.3	-12.8	32.4	22.9	14.0
^{94g}Tc ($2\alpha3n$)	83.7	55.6 ± 8.1	-37.4	-30.2	-22.8	44.1	34.2	24.9

FIG. 5. Experimentally measured FRRD of ERs (a) ^{99m}Rh, (b) ^{98}Rh, (c) ^{95g}Tc, and (d) ^{94g}Tc populated through $\alpha 2n$, $\alpha 3n$, $2\alpha 2n$, and $2\alpha 3n$ channels, respectively. The relative contributions arising from CF, ICF$^{\alpha}$, and ICF$^{2\alpha}$ processes are also mentioned in the figures. The solid lines through the data points are the Gaussian fits of the experimental data points (solid circles).
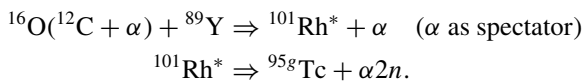
^{95g}Tc [Fig. 5(c)] correspond to the CF process. The systematics for the formation of ER ^{95g}Tc through the CF process is given by

$$^{16}O + ^{89}Y \Rightarrow {}^{105}Ag^*,$$
$$^{105}Ag^* \Rightarrow {}^{95g}Tc + 2\alpha 2n,$$
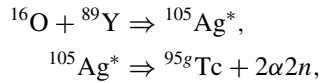
(2) ICF$^{\alpha}$ process. ICF$^{\alpha}$ process involves the fusion of ^{12}C, emerging from the α breakup of ^{16}O, with the ^{89}Y target leading to the formation of incompletely fused compound system ^{101}Rh*:

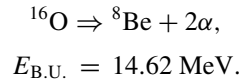$$^{16}O \Rightarrow {}^{12}C + \alpha,$$
$$E_{B.U.} = 7.16 \text{ MeV}.$$
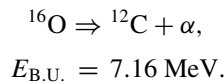
The excited intermediate compound system ^{101}Rh* will further decay via the emission of $\alpha 2n$ leading to the formation of ER ^{95g}Tc. Assuming that incident projectile ^{16}O has α cluster structure and comprises four α particles, the total incident linear momentum and energy are equally distributed among its four α constituents. Thus, ^{12}C emerging from the ^{16}O through the α breakup process is endowed with 3/4 p_{inc}. Due to a relatively lesser LMT in the case of the ICF$^{\alpha}$ process as compare to CF, ERs populated through the ICF$^{\alpha}$ process have a lesser recoil range as compared to the residues populated through the CF process. The formation of ER ^{95g}Tc through the ICF$^{\alpha}$ process may be represented as

$$^{16}O({}^{12}C + \alpha) + ^{89}Y \Rightarrow {}^{101}Rh^* + \alpha \quad (\alpha \text{ as spectator})$$
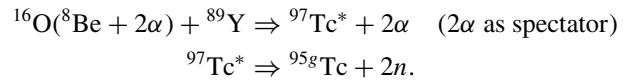$$^{101}Rh^* \Rightarrow {}^{95g}Tc + \alpha 2n.$$

The second peak in the FRRD of ^{95g}Ag [Fig. 5(c)] corresponds to the ICF$^{\alpha}$ process. Due to relatively lesser LMT, the

peak corresponding to the ICF$^{\alpha}$ process in the FRRD of ^{95g}Ag lies just before the peak corresponding to the CF process.

(3) ICF$^{2\alpha}$ process. In case of the ICF$^{2\alpha}$ process only 1/2 p_{inc} is transferred to the resulting compound system through the fusion of ^{8}Be, evolving from the 2α breakup of the incident projectile ^{16}O, with the target nucleus:

$$^{16}O \Rightarrow {}^{8}Be + 2\alpha,$$
$$E_{B.U.} = 14.62 \text{ MeV}.$$

The excited intermediate compound system ^{97}Tc*, formed through the fusion of ^{8}Be with the ^{89}Y target, further decays via the emission via the $2n$ channel leading to the formation of ERs ^{95g}Tc. As a representative case, the formation of ER ^{95g}Tc through the ICF$^{2\alpha}$ process is represented as

$$^{16}O({}^{8}Be + 2\alpha) + ^{89}Y \Rightarrow {}^{97}Tc^* + 2\alpha \quad (2\alpha \text{ as spectator})$$
$$^{97}Tc^* \Rightarrow {}^{95g}Tc + 2n.$$

The ICF$^{2\alpha}$ process leads to a transfer of only 50% of p_{inc} (1/2 p_{inc}) where as ICF$^{\alpha}$ and CF processes transfer 75% (3/4 p_{inc}) and 100% of p_{inc}, respectively, to the resulting compound system. Thus, ERs populated through the ICF$^{2\alpha}$ process recoil to the least range as compared to the residues populated through the ICF$^{\alpha}$ and CF processes. In Fig. 5(c) the peak at lowest recoil range corresponds to the ICF$^{2\alpha}$ process.

Recoil velocity and hence recoil range of the populated ERs is slightly modified by the evaporation of the nucleons and/or α particles from the intermediate compound system. Table III gives the experimentally measured (R_{expt}) as well as theoretically calculated (R_{theor}) recoil range of the observed ERs populated in the ^{16}O + ^{89}Y reaction at $E_{\text{lab}} \approx 105$ MeV. Theoretical calculations of recoil range of the observed ERs were carried out using the code Stopping and Range of Ions in Matter (SRIM) [25]. SRIM is a group of programs

TABLE III. Experimentally measured R_{expt} as well as theoretically calculated most probable range R_{theor} using the code SRIM, in Al catcher foils in units of μg/cm^2, for the experimentally observed reaction channels in the ^{16}O + ^{89}Y reaction at $E_{\text{lab}} \approx 105$ MeV.

Residue	CF		ICF$^{\alpha}$		ICF$^{2\alpha}$	
	R_{expt}	R_{theor}	R_{expt}	R_{theor}	R_{expt}	R_{theor}
^{101}Ag ($4n$)	1140 ± 64	1225				
^{101}Pd ($p3n$)	1147 ± 52	1225				
^{99}Pd ($p5n$)	1138 ± 55	1225				
^{100g}Rh (αn)	1223 ± 24	1225	810 ± 62	967		
^{99m}Rh ($\alpha 2n$)	1254 ± 35	1225	823 ± 64	967		
^{98}Rh ($\alpha 3n$)	1264 ± 23	1225	837 ± 52	967		
^{95g}Tc ($2\alpha 2n$)	1273 ± 45	1225	982 ± 32	967	647 ± 45	707
^{94g}Tc ($2\alpha 3n$)	1167 ± 42	1225	946 ± 40	967	680 ± 25	707

which calculate interaction of ions with matter. It is based on the Monte Carlo simulation method, namely the binary collision approximation with a random selection of the impact parameter of the next colliding ion. For theoretical recoil range calculations using the code SRIM, the excitation energy of the intermediate compound system is evaluated using the breakup fusion model of the ICF reaction. According to the breakup fusion model [14], the outgoing *spectator* particle (α or ^{8}Be) carries away a fraction of the incident kinetic energy and momentum proportional to its mass relative to the incident projectile. Moreover, the evaporation of nucleons and/or α particles from the recoiling intermediate compound system was found to influence the full width at half maxima (FWHM) of the FRRDs. It was observed that FWHM increase with the increase in the number of evaporated particles from the recoiling intermediate compound system, reflecting the perturbing effect of the evaporated particles on the recoil velocity of the product combined with the effect of straggling and finite target thickness.

B. Sum rule model: Exploring the role of critical angular momentum

The mechanism involved in the ICF process is still not well understood, specially in terms of angular momentum involved in the population of ERs. The study carried out by Trautmann *et al.* [26] suggests that ICF reactions are associated with peripheral collisions. On the other hand Tricoire *et al.* [27] advocates the presence of angular momentum lower than the critical value in ICF reactions. The sum rule model, given by Siwek-Wilczynska *et al.* [15], attempts to explore the role played by angular momentum in deciding the fate of compound nucleus formation through the CF or ICF process. According to the sum rule model, the ICF reaction occurs only if the angular momentum ℓ associated with the incident projectile exceeds the critical limit, called critical angular momentum ℓ_{crt}. This model assumes that partial waves, up to a hard grazing value, called the maximum angular momentum ℓ_{max}, contribute to CF or ICF and for each mode of fusion reaction there is an ℓ_{crt}, above which the incident projectile is unable to fuse with the target nucleus. Thus, ICF reactions
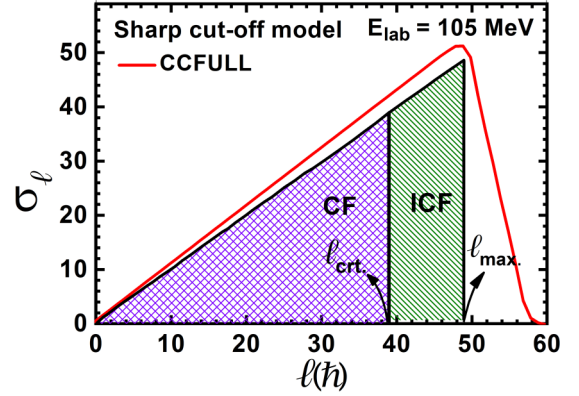

FIG. 6. Sharp cutoff approximation as well as predicted angular momentum distribution using the code CCFULL for the ^{16}O + ^{89}Y system at $E_{\text{lab}} \approx 105$ MeV. See text for details.

are localized in angular momentum space above ℓ_{crt}. At lower incident energy, ℓ_{max} is close to the ℓ_{crt}, thereby precluding any window for ICF above ℓ_{crt}.

According to Wilczynski [28] the value of ℓ_{crt} for a colliding system can be estimated from the equilibrium condition of the Coulomb, nuclear, and centrifugal forces as

$$2\pi(\gamma_1 + \gamma_2)\frac{C_1 C_2}{C_1 + C_2} = \frac{Z_1 Z_2 e^2}{(C_1 + C_2)^2} + \frac{\ell_{\text{crt}}(\ell_{\text{crt}} + 1)\hbar^2}{\mu(C_1 + C_2)}, \quad (3)$$

where C_1, C_2 are the half density radii and μ is the reduced mass of the binary system. For ℓ_{crt} less than ℓ_{max}, the maximum possible angular momentum of a system at a given incident energy, the CF cross section may be calculated as

$$\sigma_{\text{CF}} = \frac{\pi \hbar^2}{2\mu E_{\text{c.m.}}} \sum_{\ell=0}^{\ell_{\text{crt}}} (2\ell + 1) T_\ell, \quad (4)$$

where T_ℓ is the transmission coefficient for angular momentum ℓ. According to the sharp cutoff approximation [28], the transmission coefficient T_ℓ is given by

$$T_\ell = \begin{cases} 1 & \text{for } \ell \leqslant \ell_{\text{max}}. \\ 0 & \text{for } \ell > \ell_{\text{max}}. \end{cases}$$

where ℓ_{max} corresponds to peripheral collision and is given by

$$\ell_{\text{max}} = R\sqrt{2\mu(E_{\text{c.m.}} - V_B)/\hbar^2}. \quad (5)$$

Here, R is the maximum distance between two nuclei at which the collision leads to a reaction and V_B is the fusion barrier of the system at a distance R. The nature of the sharp cutoff model along with the angular momentum distribution obtained using the code CCFULL [29] are shown in Fig. 6 for the ^{16}O + ^{89}Y system at $E_{\text{lab}} \approx 105$ MeV. In order to calculate the ℓ_{crt} value using Eq. (4) the value of σ_{CF} is required. As the present work involves the offline observation of the residues, several populated ERs were not detected due to their too short half-lives. The cross section of the missing CF channels were accounted using the statistical model code PACE4 [24]. By using the code PACE4, the ratio $R = \Sigma \sigma_{xn+pxn}^{\text{PACE4}} / \sigma_{fus}^{\text{PACE4}}$ was calculated, and using this ratio the experimental CF

cross section was calculated as $\sigma_{\text{CF}}^{\text{expt}} = \Sigma \sigma_{xn+pxn}^{\text{expt}}/R$ [30]. It is necessary to mention here that value of $\sigma_{\text{CF}}^{\text{expt}}$ used in the calculation of ℓ_{crt} and ℓ_{max} as well as in the calculation of the fusion function (Sec. III C) and ICF probability (Sec. III D) is not a pure experimental CF cross section; rather, it is partly based on the statistical model code PACE4 [24]. Thus the comparisons of different data shown in Figs. 7 and 8 are not pure comparisons; rather, they are partially based on theory.

The value of ℓ_{crt} calculated using the prescription of Wilczynski *et al.* [Eq. (3)] was found to be $39\hbar$. This value of ℓ_{crt} was found to be in good agreement with the ℓ_{crt} (= $38\hbar$) value extracted from the σ_{CF} using the sharp cutoff approximation [Eq. (4)]. The value of ℓ_{max} approximated by CCFULL and PACE4 calculations (=$49\hbar$) as well as calculated using the sharp cutoff approximation (=$49\hbar$) [Eq. (5)] was found to lie sufficiently above the ℓ_{crt} value, suggesting the peripheral nature of the ICF process observed in the $^{16}\text{O} + ^{89}\text{Y}$ reaction at $E_{\text{lab}} \approx 105$ MeV.

C. Universal fusion function: Estimating the degree of fusion incompleteness

The degree of ICF contribution to the TF cross section was found to be influenced by various entrance channel parameters. It was reported by several authors [9,10,31] that CF cross section is suppressed with respect to the coupled channels (CC) calculation performed using the code CCFULL [29], which does not take into account the breakup of the incident projectile. However, the TF cross section was found to be completely reproduced by the CCFULL calculation. The extent of fusion suppression was found to governed by the $E_{\text{B.U.}}$ value of the incident projectile. In order to obtain a systematics of fusion suppression, it is necessary to eliminate (a) the static effect of the participating nuclei such as size and Coulomb barrier, and (b) the dynamic effect of the bound inelastic states and transfer coupling from the CF cross section. Thus, in order to estimate the extent of fusion incompleteness in ^{16}O induced reactions on different targets, dimensionless physical quantities, the fusion function $F(x)$, and x have been formulated as

$$F(x) = \frac{2E_{\text{c.m.}}}{R_b^2 \hbar w}\sigma_{\text{CF}}, \quad x = \frac{E_{\text{c.m.}} - V_b}{\hbar w} \quad (6)$$

using the CF cross section, as prescribed by Canto *et al.* [32]. Here R_b, V_b, and $\hbar w$ denote the radius, height, and curvature of the potential barrier, respectively. Formulation of the dimensionless variables $F(x)$ and x completely eliminates the static as well as dynamic effects between the different fusing systems and makes them comparable. The reduction of CF cross section to the fusion function $F(x)$ is derived from the Wong formula [33],

$$\sigma_{\text{CF}}(E_{\text{c.m.}}) = \frac{R_b^2 \hbar w}{2E_{\text{c.m.}}} \ln \left[1 + \exp\left(\frac{2\pi(E_{\text{c.m.}} - V_B)}{\hbar w} \right) \right]. \quad (7)$$

On simplifying the Wong formula, $F(x)$ reduces to
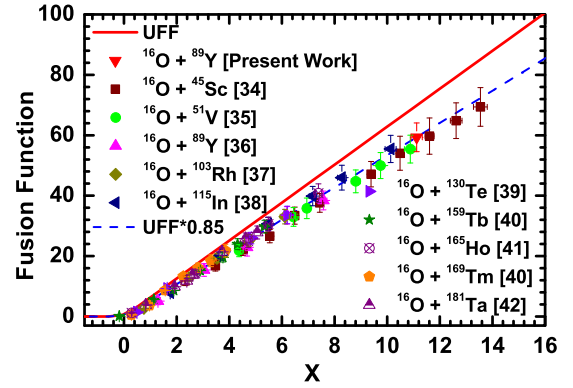
$$F_0(x) = \ln[1 + \exp(2\pi x)], \quad (8)$$

FIG. 7. The CF fusion function $F(x)$ as a function of x for the α cluster projectile ^{16}O on different targets. The solid line represents the UFF and the dotted line is the UFF multiplied by a suppression factor of 0.85.

which is known as universal fusion function (UFF). It can be noted that $F_0(x)$ is a simple function of the dimensionless variable x and is independent of the interacting system. Thus, the CF cross section data of different systems can be compared directly with the help of the UFF, and a systematics can be established. As inelastic excitation and transfer channel coupling are not so effective at energies above the Coulomb barrier, any deviation of the experimental fusion function from the UFF is attributed to the effect of projectile breakup on CF cross sections. The fusion function $F(x)$ for the α cluster projectile ^{16}O on different targets, namely ^{45}Sc [34], ^{51}V [35], ^{89}Y (present work, Ref. [36]), ^{103}Rh [37], ^{115}In [38], ^{130}Te [39], ^{159}Tb [40], ^{165}Ho [41], ^{169}Tm [40], and ^{181}Ta [42], as a function of x are illustrated in Fig. 7. For the ^{16}O projectile the most favorable breakup channel is $^{16}\text{O} \Rightarrow ^{12}\text{C} + \alpha$ with an $E_{\text{B.U.}}$ value of 7.16 MeV. In Fig. 7, the solid line represents the UFF given by Eq. (8). Suppression in the CF fusion function with respect to the UFF can be noted from Fig. 7 for all the systems. This suppression in $F(x)$ with respect to UFF is likely to arise from breakup of the ^{16}O projectile into fragments owing to its low $E_{\text{B.U.}}$ value.

D. Dependence of ICF probability on target charge

The incomplete fusion probability, defined as $P_{\text{ICF}} = \frac{\sigma_{\text{ICF}}}{\sigma_{\text{CF}} + \sigma_{\text{ICF}}}$, can be estimated by comparing the experimental fusion cross section data with the prediction of some theoretical model calculations which do not take into account the breakup of the incident projectile. The difference between the experimental and theoretical data is attributed to the ingredient missing in the theory, i.e., the breakup effect of the incident projectile. Based on this approach, a comparison of experimental fusion cross section data with the predictions of coupled channels (CC) or one-dimension barrier penetration model (1DBPM) calculations, which inherently assume that probability of compound nucleus formation $P_{\text{CN}} = 1$, has been carried out. It was observed that above the barrier energy CF cross section is suppressed as compared to the predictions of CC or 1DBPM [10,31]. The extent of fusion suppression or P_{ICF} was found to depend on various entrance channel
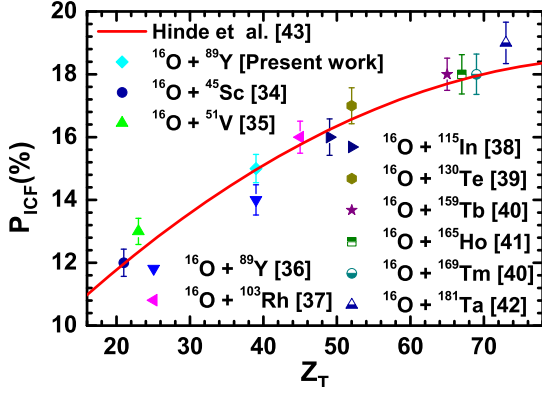
FIG. 8. Average fusion suppression as a function of Z_T for the ^{16}O induced reaction on different targets. The solid line is an empirical prediction given by Hinde *et al.* [43]. See text for details.

parameters, viz., Coulomb repulsion, breakup threshold energy of the incident projectile ($E_{B.U.}$), mass asymmetry, deformation parameter, etc.

Despite several works on fusion suppression already carried out using loosely as well as tightly bound projectiles, no systematic behavior has been observed for the variation of P_{ICF} as a function of target charge (Z_T) or mass. It is speculated that, as Z_T decreases, the role of Coulomb breakup diminishes and hence P_{ICF} decreases. There is no theoretical model proposed so far for estimating the dependence of P_{ICF} on Z_T. However, there is an empirical formula coined by Hinde *et al.* for estimating the P_{ICF} [43]. In an experiment performed using the loosely bound projectile ^{9}Be on a ^{208}Pb target, Hinde *et al.* noticed the prompt breakup of the projectile by careful analysis of the angular distribution of single and coincident α particles. The results suggest that prompt breakup of incident projectile occurs mainly due to a process occurring close to the nuclear surface. Thus, the breakup probability of the incident projectile is taken to be proportional to the gradient of nuclear potential V multiplied by an exponential factor $f(R_s)$ which is dependent on surface-to-surface separation R_s. The P_{ICF} for ^{208}Pb was then scaled to predict the P_{ICF} for any target.

Adopting the empirical formula given by Hinde *et al.* and applying it to the present system, the P_{ICF} ($= 15\%$) observed for the ^{16}O + ^{89}Y system at $E_{lab} \approx 105$ MeV is scaled to predict the P_{ICF} for the ^{16}O induced reaction on any target as

$$P_{ICF} = P_{ICF}(^{89}Y) \frac{V'_N}{V'_N(^{89}Y)} \exp\{-0.924[R_s - R_s(^{89}Y)]\}. \quad (9)$$

Here all the quantities were evaluated at the proper fusion barrier radius R_B calculated using the Sao Paulo potential [44]. The nuclear potentials for the ^{16}O + ^{89}Y system as well as for the ^{16}O induced reaction on other targets were calculated using the empirical formula prescribed by Christensen and Winther [45] as

$$V'_N = -50 \frac{R_P R_T}{R_P + R_T} \exp\left(\frac{-R_s}{0.63}\right), \quad (10)$$

where R_P, R_T, and R_s are the projectile radius, target radius, and surface-to-surface separation, respectively. The value of R_s is approximated as $R_s = R_B - R(^{16}O) - R_T$. The experimental P_{ICF} for different systems were estimated by comparing the experimental CF cross section, approximated using the method as discussed in Sec. III B, with the prediction of CC calculations performed using the code CCFULL [29]. Figure 8 shows the variation of P_{ICF} as a function of Z_T for the ^{16}O induced reaction on ^{45}Sc [34], ^{51}V [35], ^{89}Y [36], ^{103}Rh [37], ^{115}In [38], ^{130}Te [39], ^{159}Tb [40], ^{165}Ho [41], ^{169}Tm [40], and ^{181}Ta [42] targets along with the present one. As can be seen, the P_{ICF} for different systems increases monotonically with the Z_T, justifying the major role played by Coulomb repulsion in the breakup of the incident projectile.

IV. CONCLUSION

In order to estimate the degree of fusion incompleteness, the FRRDs of the observed ERs, namely ^{101}Ag ($4n$), ^{101}Pd ($p3n$), ^{99}Pd ($p5n$), ^{100g}Rh (αn), ^{99m}Rh ($\alpha 2n$), ^{98}Rh ($\alpha 3n$), ^{95g}Tc ($2\alpha 2n$), and ^{94g}Tc ($2\alpha 3n$) populated in the ^{16}O + ^{89}Y reaction at $E_{lab} \approx 105$ MeV were determined. The FRRD of ERs populated through the xn and pxn channels comprises a single peak only, suggesting a complete LMT from incident projectile to the resulting compound system through the CF process. On the other hand the FRRD of the α emitting channel residues comprises multiple peaks arising from the partial LMT through the CF, ICF$^\alpha$, and/or ICF$^{2\alpha}$ processes. The value of ℓ_{crt} extracted from the experimental CF cross section data as well as estimated theoretically using the sharp cutoff approximation was found to lie below the ℓ_{max} value, confirming the peripheral nature of the observed ICF reactions. The deduced fusion function from the CF cross section data of the present work as well as that of the ^{16}O induced reaction on different targets were compared with the UFF. It is observed that extracted fusion function for the ^{16}O induced reaction on different targets is suppressed by 15% with respect to UFF owing to the low $E_{B.U.}$ value of the incident projectile (^{16}O). The role of Coulomb breakup on P_{ICF} is explored by comparing the fusion suppression data of different ^{16}O induced reactions in light of the empirical formula suggested by Hinde *et al.* [43]. It is observed that the degree of P_{ICF} increases with the increase in charge of the target nucleus (Z_T), suggesting a major role played by Coulomb repulsion in breakup fusion reactions.

[1] S. Ali *et al.*, Eur. Phys. J. A **54**, 56 (2018).

[2] A. Agarwal *et al.*, EPJ Web Conf. **38**, 17001 (2012).

[3] F. K. Amanuel *et al.*, Phys. Rev. C **84**, 024614 (2011).

[4] H. C. Britt and A. R. Quinton, Phys. Rev. **124**, 877 (1961).

[5] H. Kumawat *et al.*, Phys. Rev. C **86**, 024607 (2012).

[6] A. Yadav *et al.*, Phys. Rev. C **86**, 014603 (2012).

[7] T. Inamura *et al.*, Phys. Lett. B **68**, 51 (1977).

[8] L. F. Canto *et al.*, Phys. Rep. **424**, 1 (2006), and the references therein.

[9] M. Dasgupta *et al.*, Phys. Rev. Lett. **82**, 1395 (1999).

[10] M. Dasgupta *et al.*, Phys. Rev. C **70**, 024606 (2004), and the references therein.

[11] P. R. S. Gomes *et al.*, Phys. Rev. C **73**, 064606 (2006).

[12] M. Blann and F. Plasil, Phys. Rev. Lett. **29**, 303 (1972).

[13] B. S. Tomar *et al.*, Phys. Rev. C **49**, 941 (1994).

[14] T. Udagawa and T. Tamura, Phys. Rev. Lett. **45**, 1311 (1980).

[15] K. Siwek-Wilczynska *et al.*, Phys. Rev. Lett. **42**, 1599 (1979).

[16] H. Tricoire *et al.*, Z. Phys. A **323**, 163 (1986).

[17] H. Morgenstern *et al.*, Phys. Rev. Lett. **52**, 1104 (1984); Z. Phys. A **313**, 39 (1983).

[18] I. Tserruya *et al.*, Phys. Rev. Lett. **60**, 14 (1988).

[19] H. E. Martz *et al.*, Nucl. Phys. A **439**, 299 (1985), and the references therein.

[20] E. Browne and R. B. Firestone, *Table of Radioactive Isotopes* (Wiley, New York, 1986).

[21] I. A. Rizvi *et al.*, Indian J. Phys. **86**, 913 (2012), and the references therein.

[22] F. K. Amanuel *et al.*, Eur. Phys. J. A **47**, 156 (2011).

[23] D. J. Parker *et al.*, Phys. Rev. C **35**, 161 (1987).

[24] A. Gavron, Phys. Rev. C **21**, 230 (1980).

[25] J. F. Ziegler, code SRIM-2006, The Stopping Power and Range of Ions in Matter, http://www.srim.org/SRIM/SRIMLEGL.htm

[26] W. Trautmann *et al.*, Phys. Rev. Lett. **53**, 1630 (1984).

[27] H. Tricoire *et al.*, Z. Phys. A **306**, 127 (1982).

[28] J. Wilczynski, Nucl. Phys. A **216**, 386 (1973).

[29] K. Hagino *et al.*, Comput. Phys. Commun. **123**, 143 (1999).

[30] C. S. Palshetkar *et al.*, Phys. Rev. C **82**, 044608 (2010).

[31] Md. Moin Shaikh *et al.*, Phys. Rev. C **91**, 034615 (2015), and the references therein.

[32] L. F. Canto *et al.*, Nucl. Phys. A **821**, 51 (2009).

[33] C. Y. Wong, Phys. Rev. Lett. **31**, 766 (1973).

[34] D. Singh *et al.*, J. Phys. Soc. Jpn. **75**, 104201 (2006).

[35] S. Mukherjee *et al.*, Eur. Phys. J. A **12**, 199 (2001).

[36] B. S. Tomar *et al.*, Z. Phys. A **343**, 223 (1992).

[37] U. Gupta *et al.*, Nucl. Phys. A **811**, 77 (2008).

[38] K. Kumar *et al.*, Phys. Rev. C **88**, 064613 (2013).

[39] D. P. Singh *et al.*, Phys. Rev. C **89**, 024612 (2014).

[40] P. P. Singh *et al.*, Phys. Rev. C **77**, 014607 (2008).

[41] K. Kumar *et al.*, Phys. Rev. C **87**, 044608 (2013).

[42] D. P. Singh *et al.*, Phys. Rev. C **80**, 014601 (2009).

[43] D. J. Hinde *et al.*, Phys. Rev. Lett. **89**, 272701 (2002).

[44] M. A. Candido Ribeiro *et al.*, Phys. Rev. Lett. **78**, 3270 (1997).

[45] P. R. Christensen and A. Winther, Phys. Lett. B **65**, 19 (1976).